RSC Advances

ROYAL SOCIETY OF CHEMISTRY

www.rsc.org/advances

Journal Name

ARTICLE

Adsorption Properties of ZrO_2 Hollow Microboxes Prepared Using $CaCO_3$ Cube as Template

Received 00th January 20xx,
Accepted 00th January 20xx

DOI: 10.1039/x0xx00000x

www.rsc.org/

Weixue Zhu, Shengsong Ge* and Qian Shao

Zirconia hollow microboxes were prepared using calcium carbonate cube as template. The as-prepared products were characterized by X-ray diffraction (XRD), scanning electron microscopy (SEM), transmission electron microscope (TEM) and nitrogen adsorption–desorption isotherms. Adsorption performance of the as-prepared products toward Congo red (CR) aqueous solutions was tested and discussed. Results show that ZrO_2 hollow microboxes copied the morphology of $CaCO_3$ template very well with a diameter of ~1.5 μm and a possible formation mechanism was proposed according to the observed results. The Langmuir surface area and BET specific surface area of ZrO_2 hollow microboxes before calcination are 301.65 m^2/g, 247.88 m^2/g, respectively and the maximum adsorbance was found to be 188.02 mg/g which is much higher than that of ZrO_2 hollow microboxes after calcination (90.86 mg/g) and ZrO_2 nanoparticles (57.86 mg/g). The adsorption kinetics and isotherms can be well described by pseudo-second order rate model and Langmuir equation, respectively. These results indicate that ZrO_2 hollow microboxes before calcination have great potential in removing dyes from water environment.

1. Introduction

With the growing rate of industrialization, huge quantities of dyes have been produced and widely used in the textile, paint, and paper industries.[1, 2] In most industrial activities, about 15% of the dyes are lost during the dyeing process and are discharged into the environment as industrial effluents, causing a serious threat to aquatic organisms and human life.[3-5] Congo red has been widely used as a kind of azo dyes owing to its superior properties such as good tinctorial strength, cheap, easy preparation, and good fastness properties.[6] However, it is highly toxic and carcinogenic without appropriate treatment before being discharged.

Dye removal from wastewater can be achieved through the following conventional methods: coagulation and flocculation, chemical oxidation, membrane separation, electrochemical processes and adsorption. Among these methods, adsorption is considered as the most recognized method for the removal of dyes present in wastewater because of its versatility, wide applicability, economic feasibility and efficient dye removal function.[7, 8] Activated carbons have been widely used as a conventional adsorbent for the treatment of wastewater. However they usually require high regeneration cost.[9, 10] In recent years, with the advances of nanoscience and technology, extensive researches to explore nanomaterials adsorbents for removing dyes are currently ongoing.[11-16] Li et al. fabricated spindle-like boehmites with high adsorption capacity for Congo red (CR) from water via a hydrothermal synthesis method.[17] Lei et al. prepared the NiO–SiO_2 hollow microspheres which were powerful adsorbents for removal of CR from water.[18] In addition, flower-like microspheres of Ni/Al mixed oxide (Ni/Al-CLDH-H) with a superior adsorption capacity has been prepared by Huang et al.[19] Many works on the synthesis of nanomaterials which have a high adsorption capacity for CR from water have been reported[20-23]. Out of several nanomaterials adsorbents reported, zirconia is one of the important materials owing to its excellent tenacity,[24] chemical stability, thermal stability,[25] corrosion resistance, high mechanical strength, and its unique adsorption performance, which have been used as nanocarriers,[26] catalysts,[27, 28] catalyst supports,[29] thermal-barrier coating, sensors,[30] and adsorbents.[31, 32]

As one of the most intriguing adsorbents, zirconia has attracted tremendous attention of researchers. Zirconia embedded in poly(ether sulfone) mixed matrix membranes (MMMs) for the removal of HA has been studied by Thuyavan et al.[33] Hornebecq et al. fabricated the mesoporous zirconia with a large specific surface area by the sol-gel process and studied its adsorption properties of CO_2.[34] Gusain et al. synthesized nanozirconia by precipitation method, and demonstrated that the nanocrystalline zirconia can be triumphantly used in the removal of chromium from aqueous solution.[35] Recently, it has already been confirmed that the

College of Chemical and Environmental Engineering, Shandong University of Science & Technology, Qingdao. Fax: +86-532-86057567; Tel: +86-532-86057567; E-mail: geshengsong@126.com

morphology of zirconia has an important influence on its properties, especially the hollow structured zirconia have superior properties. Wang et al. synthesized biomorphic ZrO_2 fibers with a better heat-insulating property by using natural silk fibers as a bio-template.[36] Wang et al. fabricated ZrO_2 hollow microsphere by a hydrothermal method and demonstrated that it exhibited a better adsorption performance for the CR from water than ZrO_2 solid microsphere and reagent samples.[37] However, the report on the synthesis of ZrO_2 hollow microboxes using $CaCO_3$ cube is not found up to now.

In this work, a novel ZrO_2 hollow microboxes were prepared using $CaCO_3$ cube as template. The adsorption capacity, kinetics adsorption for the removal of CR from water environment were studied. ZrO_2 hollow microboxes before calcination have a much better adsorption performance compared with ZrO_2 hollow microboxes after calcination and ZrO_2 nanoparticles fabricated through the same method without template.

2. Experimental

2.1 Materials

Analytical grade chemicals and reagents were used without any further purification during the experiments. Sodium carbonate (Na_2CO_3) was obtained from Tianjin Dingshengxin Chemical Co. Ltd. (Tianjin, China). Calcium chloride ($CaCl_2$) was bought from Yixing Second Chemical Reagent Co. Ltd. (Wuxi, China). Zirconium n-Butoxide (80 wt %) was purchased from Shanghai Alading Reagent Co. Ltd. (Shanghai, China). Congo red (CR) was purchased from Tianjin Damao Chemical Reagent Co. Ltd. (Tianjin, China). Deionized water and absolute alcohol were used throughout.

2.2 Preparation of $CaCO_3$ template

$CaCO_3$ cube was prepared by precipitation method at room temperature as follows: 50 mL of 0.05 M Na_2CO_3 aqueous solution was injected into the $CaCl_2$ aqueous solution with the same volume and the same concentration under ultrasound. Then the white precipitate was centrifuged and washed three times with distilled water and absolute ethanol, respectively. The $CaCO_3$ cube was obtained after drying at room temperature.

2.3 Fabrication of ZrO_2 hollow microboxes

In a typical process, 0.25 g $CaCO_3$ template was dispersed into 35 mL of the absolute ethanol by ultrasonication, followed by adding 0.125 mL distilled water under continuous magnetic stirring. Then 0.125 mL Zirconium n-Butoxide (80 wt %) was injected into the mixture. After keeping stirring for 3 h, the mixture was centrifuged and washed three times with distilled water and absolute ethanol, respectively. Then the core/shell structures were obtained by drying at room temperature followed by heating to 200 °C and maintaining for 1 h. To remove the $CaCO_3$ template, the core/shell structures were immersed in HCl (2 M) solution and washed three times with distilled water and absolute ethanol, respectively. Then, ZrO_2 hollow microboxes were obtained. ZrO_2 nanoparticles were fabricated through the same method without template for the comparison of adsorption performance. ZrO_2 hollow microboxes after calcination were obtained by calcining at 600 °C for 2 h with a ramp rate of 1 °C/min.

2.4 Characterization

Powder X-ray diffraction (XRD) patterns were recorded by a Bruker D8-Advance diffractometer (using Cu Kα= 0.1540 nm radiation) with a scanning rate of 8 °/min in 2θ range from 20°~80°. The morphology and elemental analysis of the products were examined by a field-emission scanning electron microscope (SEM, S-4800, Hitachi, Japan) fitted with an energy dispersive spectrometer (EDS) at an accelerating electron voltage of 30 kV. The microstructure of the synthesized products was investigated by a transmission electron microscope (TEM, JEM-2100, JEOL, Japan), operating at 200 kV. X-ray photoelectron spectroscopy (XPS) analyses were determined with an X-ray spectrometer K-Alpha (Thermo Scientific, USA). The surface area of the product was determined by the Brunauer-Emmett-Teller (BET) method and Langmuir method using a Micromeritics TriStar II 3020 at liquid nitrogen temperature (77 K) after the samples were dehydrated at 300 °C for 6 h.

2.5 Adsorption experiments

Adsorption kinetic experiments were carried out by adding 10 mg of products into 25 mL of 60 mg/L CR aqueous solution at room temperature, with continuous stirring. Samples were withdrawn at fixed time intervals, and the adsorbents were separated by centrifugation. The absorption spectrum of residual dyes was determined using UV-vis spectrophotometer (UV-vis DRS, UH4150, Hitachi, Japan) at 497 nm, corresponding to the maximum absorption wavelengths of the CR. The standard curve was made by determining the absorbance of each standard solution in order to calculate residual dye concentrations.

The adsorbance of CR dyes at any time (Q_t (mg/g)) was calculated using the following equations:

$$Q_t = \frac{(C_0 - C_t)V}{W} \quad (1)$$

where C_0 (mg/L) are the initial dye concentration, V is the volume of the CR solution (L), and W is the mass of adsorbent used (g).

Adsorption isotherm experiments were carried out by following the adsorption for the standard solution of the CR dye. The experimental process was as described below: 10 mg samples were dispersed in a series of 100 mL stoppered conical flask which containing 25 mL of CR aqueous solution with different initial concentrations (20 to 240 mg/L), and the experiments were carried out at room temperature for 12 h with continuous stirring to ensure equilibrium. After adsorption reaching equilibrium, the adsorbent was separated

by centrifugation at 10000 rpm for several minutes. The absorption spectrum of residual dyes in the solution was measured with UV-vis spectrophotometer.

The adsorbance of CR dyes at adsorption equilibrium (Q_e (mg/g)) was calculated using the following equations:

$$Q_e = \frac{(C_0 - C_e)V}{W} \quad (2)$$

where C_e (mg/L) are the equilibrium concentration, V is the volume of the CR solution (L), and W is the mass of adsorbent used (g).

3. Results and discussion

3.1 XRD analysis

Crystallinity and crystalline phase of the as-prepared samples were determined with X-ray diffractometer (XRD), as shown in Fig.1. The XRD results testify that the as-prepared samples before calcination were amorphous, and four main peaks of the samples after calcination at 600 °C were characteristic of the tetragonal phase of ZrO_2 (JCPDS card: 79-1769)[38, 39] which could prove that the hollow microboxes before calcination were ZrO_2. The XRD patterns of ZrO_2 nanoparticles before and after calcination are the same as that of hollow ZrO_2 microboxes.

3.2 XPS analysis

The XPS spectra of ZrO_2 hollow microboxes before and after calcination are presented in Fig.2. The binding energy peak of O 1s for both samples were at 529.2 eV (Fig.2a) and 531.6 eV (Fig.2c), respectively. Fig.2b and 2d present the spectra for Zr 3d of ZrO_2 hollow microboxes before and after calcination, respectively. The binding energy peaks located at 183.58 eV and 181.08 eV can be assigned to Zr $3d_{5/2}$ and the peaks at 185.78 eV and 183.48 eV can be assigned to Zr $3d_{3/2}$ for the Zr^{4+} state, indicating the main valence of zirconium in the ZrO_2 product is +4.[40]

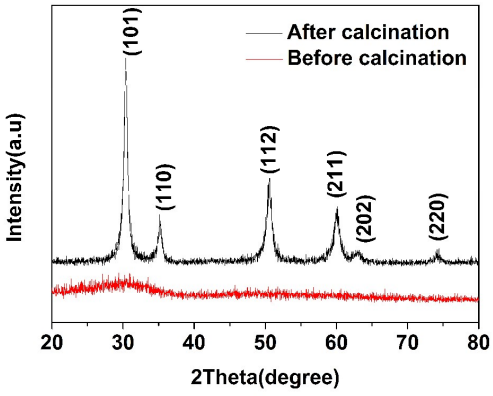

Fig.1 XRD pattern of ZrO_2 hollow microboxes.

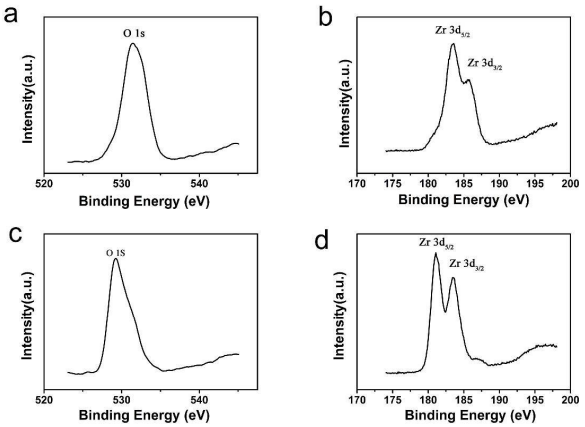

Fig.2 The XPS survey spectra of ZrO_2 hollow microboxes before(a,b) and after(c,d) calcination.

3.3 SEM analysis

SEM images of $CaCO_3$ template are shown in Fig.3a and Fig.3b, which illustrate that the $CaCO_3$ template is cubic in morphology with a uniform particle size of ~1.5 μm, and the surface of $CaCO_3$ is consisted of terraces.[41] Fig.3c and Fig.3d show the SEM images of ZrO_2 hollow microboxes before calcination, which indicate ZrO_2 hollow microboxes retain the cubic morphology and terraced surface of $CaCO_3$ template. Furthermore, the hollow structure can be clearly observed from the broken microboxes which are caused by the escapement of CO_2 during the removing of $CaCO_3$ template.

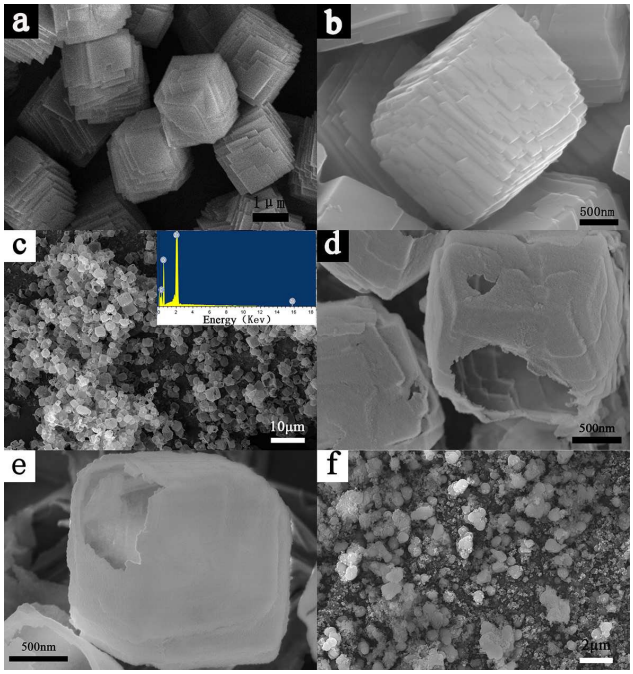

Fig.3 SEM images of $CaCO_3$ template (a, b), ZrO_2 hollow microboxes before (c, d) and after (e) calcination, ZrO_2 (f) nanoparticles.

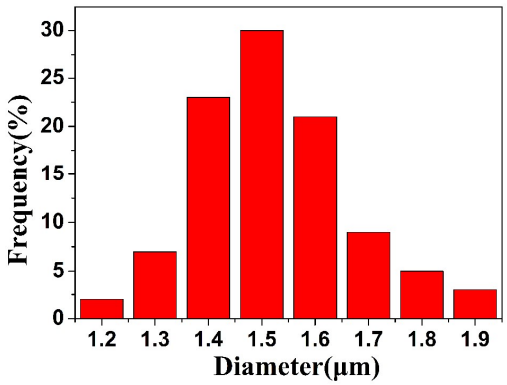

Fig.4 Particle size distribution of ZrO_2 hollow microboxes.

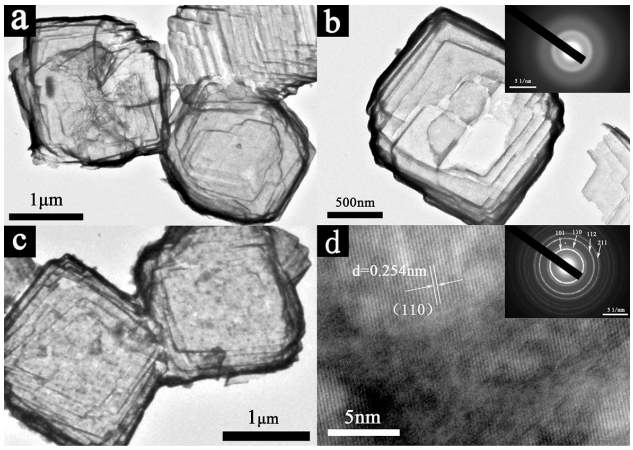

Fig.5 TEM images of ZrO_2 hollow microboxes before (a,b) and after (c) calcination, HRTEM image of zirconia hollow microboxes after calcination (d).

Fig.3e shows the SEM image of ZrO_2 hollow microboxes after calcination, which indicates the products retain the hollow structure after calcination at 600 °C. Fig.3f shows the SEM image of ZrO_2 nanoparticles, which indicates the morphology of ZrO_2 nanoparticle is irregular and the size is not uniform, and the serious aggregation can be observed. Fig.3c inset shows the EDS spectra of ZrO_2 hollow microboxes before calcination. The EDS spectra indicate that ZrO_2 hollow microboxes before calcination are composed of Zr and O elements, and the EDS spectra of ZrO_2 hollow microboxes after calcination and ZrO_2 nanoparticles are the same as that of ZrO_2 hollow microboxes before calcination.

The particle size distribution (Fig. 4) of ZrO_2 hollow microboxes was studied by surveying 100 particles from the SEM images. It can be evidently seen that the particle size has a narrow distribution with a uniform particle size of ~1.5 μm and the particle size is mostly in the range of 1–2 μm.

3.4 TEM analysis

Fig.5a and Fig.5b shows the representative TEM micrographs of ZrO_2 hollow microboxes before calcination. The cubic structure of hollow ZrO_2 with distinct darker lines as walls is clearly observed, and the shell thickness of the ZrO_2 hollow microboxes is about 35 nm which is consistent with the SEM images. Fig.5c shows the TEM image of hollow ZrO_2 after calcination which indicates that the products after calcination retain the morphology of hollow microboxes. The high resolution transmission electron microscopy (HRTEM) image of ZrO_2 hollow microboxes after calcination is shown in Fig.5d and the well-defined lattice planes are observed which indicate the high crystallinity of the tetragonal zirconia microboxes. The diffraction ring of selected area electron diffraction (SAED) of ZrO_2 hollow microboxes before calcination (Fig.5b inset) is not clear which indicates the product is amorphous. SAED of ZrO_2 hollow microboxes after calcination is shown in Fig.5d inset. Both SAED results are well consistent with XRD pattern.

3.5 Formation mechanism

The possible formation process of ZrO_2 hollow microboxes could be predicted on the basis of information obtained, as shown in Fig.6. It can be concluded in four subsequent steps. In the first step, the $Zr(OH)_4$ shell was formed on the surface of $CaCO_3$ cube by the hydrolysis of zirconium n-butoxide. In the second step, the $Zr(OH)_4$ shell transformed into amorphous ZrO_2 by heating to 200 °C and maintaining for 1 h. In the next step, the core/shell structures were immersed into 2M HCl to removing the $CaCO_3$ template, and amorphous ZrO_2 hollow microboxes were fabricated. No product was left without the second-step after removing the $CaCO_3$ template, which could prove that the hydrolysate of zirconium n-butoxide was $Zr(OH)_4$. Finally, tetragonal zirconia hollow microboxes were obtained after calcination at 600 °C of the amorphous ZrO_2.

3.6 Nitrogen adsorption-desorption isotherms

Fig.7 shows the N_2 adsorption–desorption isotherms of the as-prepared samples. The BET specific surface areas and Langmuir specific surface areas of the three samples are shown in Table 1. The results indicate that the specific surface areas of products before calcination are much larger than that of products after calcination. This might be attributed to the amorphous phase

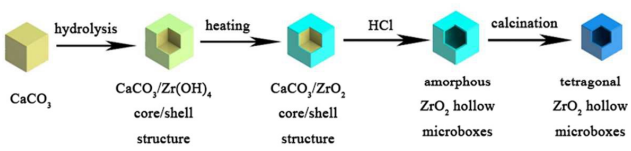

Fig.6 Schematic mechanism toward using $CaCO_3$ as template for ZrO_2 hollow microboxes.

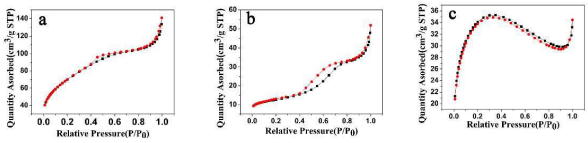

Fig.7 Nitrogen adsorption–desorption isotherms of the ZrO_2 hollow microboxes before(a) and after(b) calcination and ZrO_2 nanoparticles(c).

Table 1. BET specific surface areas and Langmuir specific surface areas of ZrO_2 microboxes before(a) and after(b) calcination and ZrO_2 nanoparticles(c).

Samples	BET specific surface areas (m^2/g)	Langmuir specific surface areas (m^2/g)
a	247.88	301.65
b	44.23	54.49
c	122.47	151.74

of the products before calcination. Meanwhile, the specific surface areas of ZrO_2 hollow microboxes before calcination are much larger than that of ZrO_2 nanoparticles, which might be caused by the hollow structure.

3.7 Adsorption performance

3.7.1 Adsorption kinetic experiments

Fig.8 shows the CR adsorption kinetics of ZrO_2 hollow microboxes before (a) and after (b) calcination and ZrO_2 nanoparticles (c). The adsorbance of samples increase sharply during the first 20 min and then level off as equilibrium is achieved. The equilibrium adsorbance of ZrO_2 hollow microboxes before and after calcination and ZrO_2 nanoparticles are 132.69 mg/g, 81.58 mg/g, and 55.26 mg/g, respectively. Compared with ZrO_2 nanoparticles, the Langmuir specific surface area of ZrO_2 hollow microboxes before calcination is much larger than that of ZrO_2 nanoparticles, but the adsorbance is not proportional to the Langmuir specific surface area, although they have the same crystal shape. This might be attributed to the different morphology. So the hollow structure can promote the adsorption performance of the adsorbents. Meanwhile, although the Langmuir specific surface area of ZrO_2 hollow microboxes before calcination is much larger than that of ZrO_2 hollow microboxes after calcination, the adsorbance is also not proportional to the Langmuir specific surface area. This might be caused by the different crystal shape, therefore the tetragonal phase of samples is benificial to the adsorption performance compared with amorphous phase. ZrO_2 nanoparticles, which have neither hollow structure nor tetragonal phase, have a poor adsorption performance, although with a larger specific surface area compared with ZrO_2 microboxes after calcination. The result further confirms that specific surface area is not the only factor influencing adsorption performance, the crystal shape and morphology also play important roles in adsorption performance.

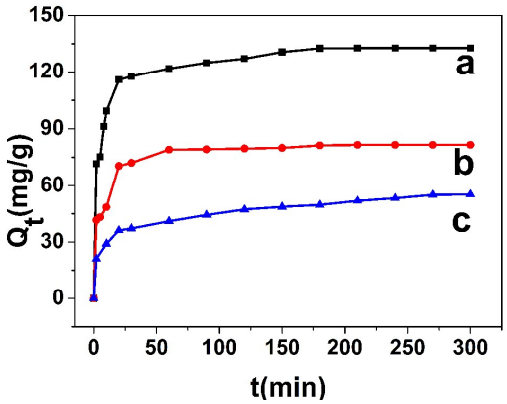

Fig.8 Adsorption kinetics for CR adsorption on ZrO_2 hollow microboxes before(a) and after(b) calcination and ZrO_2 nanoparticles(c).

In the present study, pseudo-first-order and pseudo-second-order kinetic models have been applied to investigate adsorption kinetics of ZrO_2 hollow microboxes before and after calcination and ZrO_2 nanoparticles. The pseudo-first-order and pseudo-second-order rate equations are given as follows:

$$\ln(Q_e - Q_t) = \ln Q_e - K_1 t \quad (3)$$

$$\frac{t}{Q_t} = \frac{1}{K_2 Q_e^2} + \frac{t}{Q_e} \quad (4)$$

Where Q_e and Q_t are the adsorbance of CR dyes at adsorption equilibrium and at any time t, respectively, K_1 (min^{-1}) is the pseudo-first-order rate constant, K_2 (g/(mg·min)) is the pseudo-second-order rate constant.

Table 2 has summarized the adsorption kinetic constants and correlation coefficients (R^2) of the pseudo-first-order and

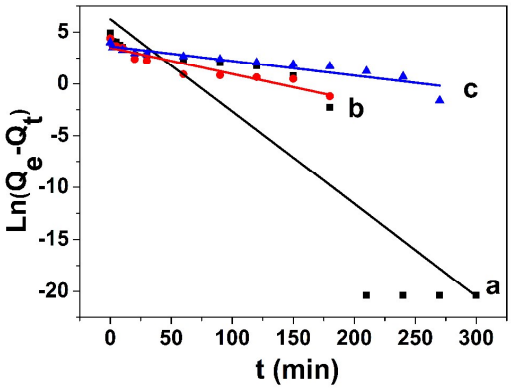

Fig.9 Pseudo-first-order kinetics isotherms for CR adsorption on ZrO_2 hollow microboxes before(a) and after(b) calcination and ZrO_2 nanoparticles(c).

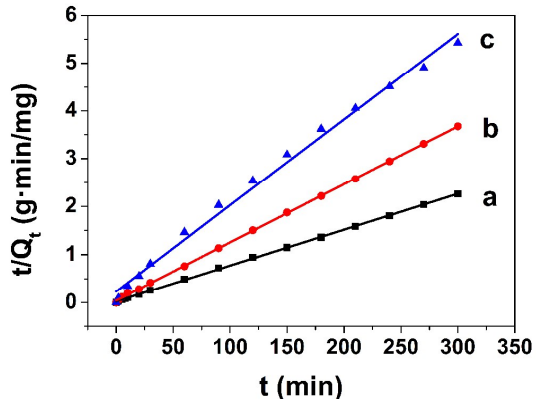

Fig.10 Pseudo-second-order kinetics isotherms for CR adsorption on ZrO_2 hollow microboxes before(a) and after(b) calcination and ZrO_2 nanoparticles(c).

pseudo-second-order models. The value of K_1 and K_2 are calculated from the plots in Fig.9 and Fig.10, respectively. It is clear that pseudo-first-order models are not suitable to describe the kinetic profile because of R^2 are relatively small. Conversely, the R^2 of three samples from the pseudo-second-order kinetic model are greater than 0.99 and the theoretical Q_e value calculated from the pseudo-second-order kinetic models are close to the experimental value, which indicates the pseudo-second-order mechanism is predominant.

3.7.2 Adsorption isotherm experiments

The adsorption isotherms of ZrO_2 microboxes before (a) and after (b) calcination and ZrO_2 nanoparticles (c) are shown in Fig.11. It can be seen that the maximum adsorbance of samples increased continually with the increase of concentration, and finally achieved a maximum equilibrium adsorbance. The maximum adsorbance of ZrO_2 hollow microboxes before and after calcination and ZrO_2 nanoparticles are 188.02 mg/g, 90.86 mg/g, and 57.86 mg/g, respectively.

In this study, two mostly used models, namely Langmuir and Freundlich, were used to analyze the experimental data. The Langmuir and Freundlich isotherms are represented, respectively, by:

$$\frac{C_e}{Q_e} = \frac{C_e}{Q_m} + \frac{1}{K_L Q_m} \quad (5)$$

$$\log Q_e = \log K_F + \frac{1}{n}\log C_e \quad (6)$$

where Q_m (mg/g) is the maximum adsorbance, K_L (L/mg) is the Langmuir constant, and K_F and n ($mg^{(1-(1/n))}\cdot L^{(1/n)}/g$) are Freundlich constants.

Table 3 displays the fitting results for the adsorption of ZrO_2 hollow microboxes before and after calcination and ZrO_2 nanoparticles (see Fig.12 and Fig.13). The fitting results show that Langmuir model is better fit the isotherm data with a higher R^2 compared with Freundlich model. It implies that the adsorption of the sorbents is homogeneous. Moreover, the theoretical Q_m values calculated from the Langmuir model are found to be 203.25 mg/g, 94.97 mg/g, and 58.86 mg/g for ZrO_2 hollow microboxes before and after calcination and ZrO_2 nanoparticles, respectively, which are close to the experimental values of Q_m.

4. Conclusions

In summary, zirconia hollow microboxes with a diameter of ~1.5 μm and thickness of ~35 nm were successfully synthesized using calcium carbonate cube as template. The CR

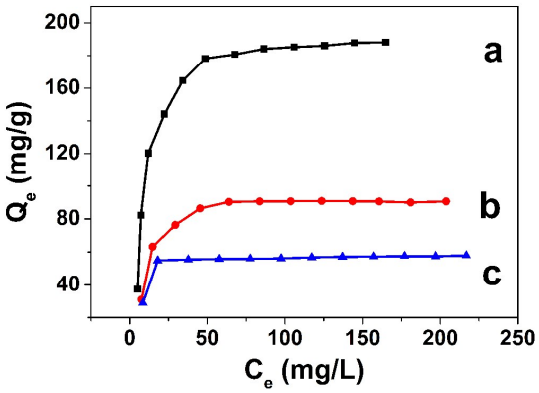

Fig.11 Adsorption isotherms for CR adsorption on ZrO_2 hollow microboxes before(a) and after(b) calcination and ZrO_2 nanoparticles(c).

Table 2. Pseudo-first-order kinetics and the pseudo-second-order kinetics isotherm constants of CR adsorption on ZrO_2 microboxes before(a) and after(b) calcination and ZrO_2 nanoparticles(c).

Samples	Experimental values	Pseudo-first-order kinetics			Pseudo-second-order kinetics		
	Q_e (mg/g)	Q_e (mg/g)	K_1 (min^{-1})	R^2	Q_e (mg/g)	K_2 (g/(mg·min))	R^2
a	132.69	511.34	0.0890	0.808	134.23	0.0020	0.999
b	81.58	33.31	0.0254	0.873	82.64	0.0034	0.999
c	55.26	37.68	0.0141	0.847	55.80	0.0014	0.993

Journal Name

ARTICLE

Table 3. Langmuir and Freundlich isotherm constants of CR adsorption on ZrO_2 hollow microboxes before (a) and after (b) calcination and ZrO_2 nanoparticles(c).

Samples	Experimental values	Langmuir isotherm model			Freundlich isotherm model		
	Q_m (mg/g)	Q_m (mg/g)	K_L (L/mg)	R^2	n ($mg^{(1-(1/n))}\cdot L^{(1/n)}/g$)	K_F ($mg^{(1-(1/n))}\cdot L^{(1/n)}/g$)	R^2
a	188.02	203.25	0.0926	0.994	2.851	38.09	0.726
b	90.86	94.97	0.1388	0.997	3.961	27.28	0.682
c	57.86	58.86	0.2409	0.999	6.993	28.71	0.512

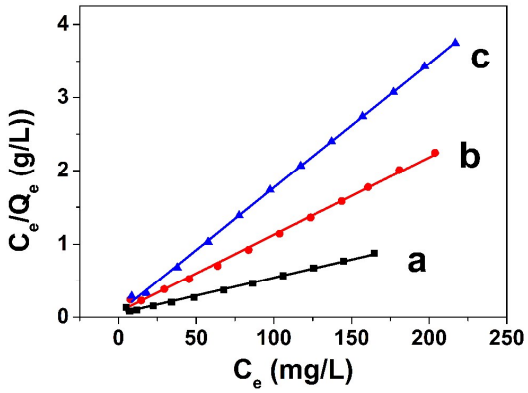

Fig.12 Langmuir isotherms for CR adsorption on ZrO_2 hollow microboxes before(a) and after(b) calcination and ZrO_2 nanoparticles(c).

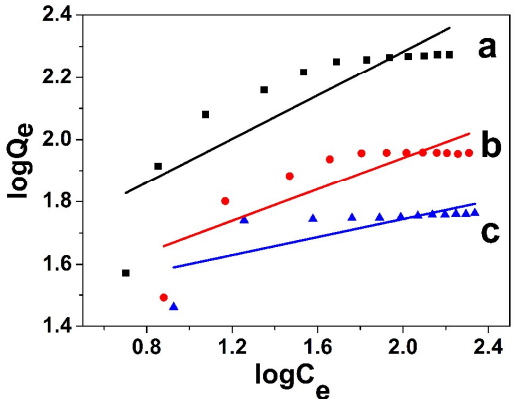

Fig.13 Freundlich isotherms for CR adsorption on ZrO_2 hollow microboxes before(a) and after(b) calcination and ZrO_2 nanoparticles(c).

adsorption isotherms of products can be well described by the Langmuir isotherms equation, and the adsorption kinetics can be well-fitted with the pseudo-second-order model. Zirconia hollow microboxes demonstrate a much higher adsorbance (188.02 mg/g) than ZrO_2 hollow microboxes after calcination (90.86 mg/g) and ZrO_2 nanoparticles (57.86 mg/g). These results indicate that ZrO_2 hollow microboxes are beneficial for the removal of the dyes from a watery environment.

Acknowledgements

The authors wish to acknowledge Shangrao Boshiming Chemical Co. Ltd (Shangrao, China) for financial support of this study. The authors would also like to express their gratitude towards Zhaofeng He for his technical assistance.

Notes and references

1 W.-H. Leung, W.-H. Lo and P.-H. Chan, *RSC Adv.*, 2015, **5**, 90022-90030.
2 S. K. Das, M. M. Khan, T. Parandhaman, F. Laffir, A. K. Guha, G. Sekaran and A. B. Mandal, *Nanoscale*, 2013, **5**, 5549-5560.
3 M. Arshadi, F. SalimiVahid, J. W. L. Salvacion and M. Soleymanzadeh, *RSC Advances*, 2014, **4**, 16005.
4 K. Selvam, K. Swaminathan and K. S. Chae, *Bioresource* technology, 2003, **88**, 115-119.
5 T. Bhowmik, M. K. Kundu and S. Barman, *RSC Adv.*, 2015, **5**, 38760-38773.
6 A. Ahmad, S. H. Mohd-Setapar, C. S. Chuong, A. Khatoon, W. A. Wani, R. Kumar and M. Rafatullah, *RSC Adv.*, 2015, **5**, 30801-30818.
7 P. Z. Ray and H. J. Shipley, *RSC Adv.*, 2015, **5**, 29885-29907.

8 M. Yusuf, F. M. Elfghi, S. A. Zaidi, E. C. Abdullah and M. A. Khan, RSC *Adv.*, 2015, **5**, 50392-50420.
9 P. Wang, Q. Shi, Y. Shi, K. K. Clark, G. D. Stucky and A. A. Keller, *Journal of the American Chemical Society*, 2009, **131**, 182-188.
10 Z. H. *Sun*, L. F. Wang, P. P. Liu, S. C. Wang, B. Sun, D. Z. Jiang and F. S. Xiao, *Advanced Materials*, 2006, **18**, 1968-1971.
11 J. Hu, Z. Song, L. Chen, H. Yang, J. Li and R. Richards, Journal *of Chemical & Engineering Data*, 2010, **55**, 3742-3748.
12 J. Y. Luo, Y. R. Lin, B. W. Liang, Y. D. Li, X. W. Mo and Q. G. Zeng, *RSC Adv.*, 2015, **5**, 100898-100904.
13 O. V. Kharissova, H. V. R. Dias and B. I. Kharisov, *RSC Adv.*, 2015, **5**, 6695-6719.
14 S. Banerjee, R. K. Gautam, A. Jaiswal, M. Chandra Chattopadhyaya and Y. Chandra Sharma, *RSC Adv.*, 2015, **5**, 14425-14440.
15 H. Sun, L. Cao and L. Lu, *Nano Research*, 2011, **4**, 550-562.
16 A. Ghosal, J. Shah, R. K. Kotnala and S. Ahmad, *Journal of* Materials *Chemistry A*, 2013, **1**, 12868.
17 G. Li, Y. Sun, X. Li and Y. Liu, *RSC Adv.*, 2016, **6**, 11855-11862.
18 C. Lei, X. Zhu, B. Zhu, J. Yu and W. Ho, *Journal of colloid and interface science*, 2016, **466**, 238-246.
19 W. Huang, X. Yu and D. Li, *RSC Adv.*, 2015, **5**, 84937-84946.
20 X.-J. Jia, J. Wang, J. Wu, Y. Du, B. Zhao and D. d. Engelsen, *RSC Adv.*, 2015, **5**, 72321-72330.
21 B. Ding, C. Guo, S. X. Liu, Y. Cheng, X. X. Wu, X. M. Su, Y. Y. Liu and Y. Li, *RSC* Adv., 2016, **6**, 33888-33900.
22 C. Lei, X. Zhu, Y. Le, B. Zhu, J. Yu and W. Ho, *RSC Adv.*, 2016, **6**, 10272-10279.
23 S. Dhanavel, E. A. K. Nivethaa, K. Dhanapal, V. K. Gupta, V. Narayanan and A. Stephen, *RSC Adv.*, 2016, **6**, 28871-28886.
24 X. Liu, C. Kan, X. Wang, X. Yang and L. Lu, *Journal of the American Chemical Society*, 2006, **128**, 430-431.
25 X. M. Liu, G. Q. Lu and Z. F. Yan, *The Journal of Physical Chemistry B*, 2004, **108**, 15523-15528.
26.G. Sponchia, E. Ambrosi, F. Rizzolio, M. Hadla, A. D. Tedesco, C. R. Spena, G. Toffoli, P. Riello and A. Benedetti, *J. Mater. Chem. B*, 2015, **3**, 7300-7306.
27.I. M. Hill, S. Hanspal, Z. D. Young and R. J. Davis, *The Journal of Physical* Chemistry *C*, 2015, **119**, 9186-9197.
28.Z.-Y. Lim, C. Wu, W. G. Wang, K.-L. Choy and H. Yin, *J. Mater. Chem. A*, 2016, **4**, 153-159.
29 Z. Jin, F. Wang, F. Wang, J. Wang, J. C. Yu and J. Wang, Advanced *Functional Materials*, 2013, **23**, 2137-2144.
30 E. Pena dos Santos, C. V. Santilli, S. H. Pulcinelli and E. Prouzet, *Chemistry of Materials*, 2004, **16**, 4187-4192.
31 K. Pokrovski, K. T. Jung and A. T. Bell, *Langmuir*, 2001, **17**, 4297-4303.
32 C. Morterra, G. Cerrato, E. Novarino and M. Peñarroya Mentruit, *Langmuir*, 2003, **19**, 5708-5721.
33 Y. L. Thuyavan, N. Anantharaman, G. Arthanareeswaran and A. F. Ismail, Industrial *& Engineering Chemistry Research*, 2014, **53**, 11355-11364.
34 V. Hornebecq, C. Knöfel, P. Boulet, B. Kuchta and P. L. Llewellyn, *The* Journal *of Physical Chemistry C*, 2011, **115**, 10097-10103.
35 D. Gusain, F. Bux and Y. C. Sharma, *Journal of Molecular Liquids*, 2014, **197**, 131-141.
36 T. Wang, S. Kong, L. Chang and C. Wong, *Ceramics International*, 2012, **38**, 6783-6788.
37 C. Wang, Y. Le and B. Cheng, *Ceramics International*, 2014, **40**, 10847-10856.
38 P. A. Deshpande, S. Polisetti and G. Madras, *Langmuir*, 2011, **27**, 3578-3587.
39 D. Gusain, S. N. Upadhyay and Y. Chandra Sharma, *RSC* Advances, 2014, **4**, 18755.
40 J. L. Clabel H, V. A. G. Rivera, M. Siu Li, L. A. O. Nunes, E. R. Leite, W. H. Schreiner and E. Marega, *Journal of Alloys and Compounds*, 2015, **619**, 800-806.
41 K. Rae Cho, Y. Y. Kim, P. Yang, W. Cai, H. Pan, A. N. Kulak, J. L. Lau, P. Kulshreshtha, S. P. Armes, F. C. Meldrum and J. J. De Yoreo, *Nature communications*, 2016, **7**, 10187.

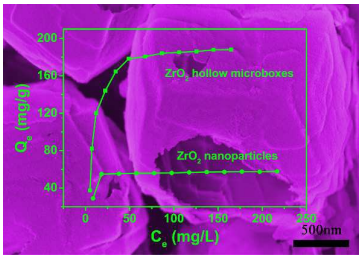

ZrO_2 hollow microboxes prepared using $CaCO_3$ cube as template exhibit excellent dye adsorption performance from wastewater.